

# Real-Time Non-Smooth MPC for Switching Systems: Application to a Three-Tank Process

Hendrik Alsmeier<sup>1</sup>, Felix Häusser<sup>1</sup>, Andreas Knödler<sup>1</sup>, Armin Nurkanović<sup>2</sup>, Anton Pozharskiy<sup>2</sup>,  
Moritz Diehl<sup>2</sup>, and Rolf Findeisen<sup>1</sup>

**Abstract**—Real-time model predictive control of non-smooth switching systems remains challenging due to discontinuities and the presence of discrete modes, which complicate numerical integration and optimization. This paper presents a real-time feasible non-smooth model predictive control scheme for a physical three-tank process, implemented without mixed-integer formulations. The approach combines Filippov system modeling with finite elements and switch detection for time discretization, leading to a finite-dimensional optimal control problem formulated as a mathematical program with complementarity constraints. The mathematical program is solved via a homotopy of smooth nonlinear programs. We introduce modeling adjustments that make the three-tank dynamics numerically tractable, including additional modes to avoid non-Lipschitz points and undefined function values. Hardware experiments demonstrate efficient handling of switching events, mode-consistent tracking across reference changes, correct boundary handling, and constraint satisfaction. Furthermore, we investigate the impact of model mismatch and show that the tracking performance and computation times remain within real-time limits for the chosen sampling time. The complete controller is implemented using the non-smooth optimal control framework NOSNOC.

## I. INTRODUCTION

Many real-world systems combine continuous physical dynamics with discrete switching events, for example, due to valve operations in process units or contact and friction phenomena in mechanical systems. Such behavior is naturally described by models that are only piecewise smooth, exhibiting non-smooth dynamics at region boundaries [1].

Model predictive control (MPC) is a well-established and reliable control strategy that profits from the use of high-fidelity models [2], [3]. However, for systems that are only piecewise smooth, the discontinuities at region boundaries pose challenges for numerical integration and optimization, significantly increasing computational complexity [1].

Commonly, switching behavior in MPC is handled by encoding the modes explicitly using the mixed logical dynamical (MLD) framework [4], [5], which leads to mixed-integer optimal control problems. This formulation preserves the switching structure by design and has been extensively studied in terms of modeling, stability, and applications.

However, solving mixed-integer problems online is computationally demanding for fast sampling times and non-trivial horizons [4]–[7], and nonlinearities further increase the number of integer variables required. Recent progress has improved warm-started branch-and-bound methods for hybrid MPC, including results on a three-tank benchmark [8].

In addition to mixed-integer formulations, continuous-time approaches based on non-smooth analysis and Filippov theory provide a rigorous description of switching dynamics. However, standard smooth-MPC formulations are not well suited for such systems: sensitivities become ill-defined near switching boundaries, and numerical integration may fail to preserve the underlying mode changes [3], [9]. In practice, preserving the switching logic while achieving real-time feasibility with acceptable model accuracy is often challenging. Smoothing or regularization can improve tractability but generally degrades constraint satisfaction and yields inconsistent sensitivities at switching boundaries [10], [11]. The non-smooth optimal control framework (NOSNOC) introduced in [12] uses finite elements with switch detection (FESD) [13] to discretize non-smooth systems. This transcribes the resulting optimal control problems into mathematical programs with complementarity constraints (MPCCs). The arising MPCCs can be solved efficiently using regularization–homotopy methods, cf. [14]. The FESD approach resolves sensitivity issues near switching boundaries by aligning discretization nodes with switching events, keeping the active set constant within each finite element, and solving the resulting complementarity-constrained nonlinear programs (NLPs) without using integer variables [13], [15].

*Contributions.* In this work, we present an MPC formulation based on the NOSNOC framework and report, to the best of our knowledge, the first real-time closed-loop implementation on a physical three-tank system exhibiting switching behavior due to inter-tank flows and drains. The proposed controller preserves the switching logic and implicitly detects mode transitions via the FESD discretization, ensuring consistent mode sequencing and correct sliding behavior without relying on mixed-integer formulations. We demonstrate closed-loop tracking performance, constraint satisfaction, and real-time computation under varying references, confirming the feasibility of a continuous-optimization pipeline from CasADi [16] through NOSNOC to IPOPT [17].

*Outline.* Section II formalizes the piecewise-smooth model and Filippov inclusion for the three-tank system. Thereafter, Section III presents the NOSNOC MPC formulation, the FESD discretization, and the resulting MPCC. Section IV

<sup>1</sup>Control and Cyber-Physical Systems Laboratory (CCPS), Technical University of Darmstadt, Germany. {hendrik.alsmeier, felix.haeusser, rolf.findeisen}@iat.tu-darmstadt.de, andreas.knoedler@mail.de

<sup>2</sup>Department of Microsystems Engineering (IMTEK), University of Freiburg, Germany. {armin.nurkanovic, anton.pozharskiy, moritz.diehl}@imtek.uni-freiburg.de

This research was supported by DFG via projects 504452366 (SPP 2364) and 525018088, by BMWK via 03EI4057A and 03EN3054B, and by the DLR via 20E2219B.

reports hardware experiments and simulation studies, and Section V concludes with limitations and directions for further development.

## II. PROBLEM SETUP

We consider a continuous-time nonlinear system

$$\dot{x}(t) = f(x(t), u(t)), \quad (1)$$

with  $x(t) \in \mathbb{R}^{n_x}$ ,  $u(t) \in \mathbb{R}^{n_u}$ . For brevity, we will forgo the time dependents for  $x$  and  $u$  in the following if it is not specifically relevant. In this work,  $f : \mathbb{R}^{n_x} \times \mathbb{R}^{n_u} \rightarrow \mathbb{R}^{n_x}$  is piecewise-smooth function. Thus, we assume there exist disjoint, nonempty, connected, locally finite, open regions  $\{R_i\}_{i=1}^m$  with closure  $\bar{R}_i$  and piecewise-smooth boundaries  $\partial R_i$  such that  $\bigcup_{i=1}^m R_i = \mathbb{R}^{n_x} \setminus \Gamma$  with  $\Gamma := \bigcup_{i=1}^m \partial R_i$  of Lebesgue measure 0. For each mode  $i \in \{1, \dots, m\}$ , let  $f_i : \mathbb{R}^{n_x} \times \mathbb{R}^{n_u} \rightarrow \mathbb{R}^{n_x}$  be smooth on an open neighborhood of  $\bar{R}_i$ . Thus, we define the piecewise-smooth system  $f$  as [12]

$$f(x, u) := f_i(x, u) \quad \text{if } x \in R_i, i \in \{1, \dots, m\}. \quad (2)$$

In general, the dynamics are not defined on the boundaries  $\partial R_i$ , which may introduce discontinuities. This presents issues for model-based and gradient-based control approaches like MPC, as gradients and solution sensitivities are ill-defined on the boundaries, and transitioning between mutually exclusive dynamics is nontrivial [4], [9], [12]. To obtain a well-posed model at the boundaries, we use the Filippov differential inclusion (FDI) [18]

$$\dot{x} \in F(x, u) := \left\{ \sum_{i=1}^m \theta_i f_i(x, u) \mid \sum_i \theta_i = 1, \theta_i \geq 0, \theta_i = 0 \text{ if } x \notin \bar{R}_i \right\}. \quad (3)$$

Here  $\theta_i$  are functions used as convex multipliers for  $F : \mathbb{R}^{n_x} \times \mathbb{R}^{n_u} \rightrightarrows \mathbb{R}^{n_x}$ . In the interior of  $R_i$ , the dynamics reduce to  $F(x, u) = \{f_i(x, u)\}$ . On boundaries,  $F(x, u)$  is the convex combination of vector fields of the neighboring regions  $R_i$  [12], [18]. This recasting of the dynamics as the FDI (3) yields a well-posed continuous-time model. This model can be used to formulate a non-smooth Optimal Control Problem (OCP) and derive a real-time MPC scheme tailored to this structure.

## III. NON-SMOOTH MPC VIA NOSNOC

### A. MPC formulation

Given the Filippov model  $\dot{x} \in F(x, u)$ , we pose the continuous-time OCP on a horizon  $[0, T]$ ,  $T > 0$  [12]:

$$\min_{x(\cdot), u(\cdot)} \int_0^T \ell(x(t), u(t)) dt + \ell_T(x(T)) \quad (4a)$$

$$\text{s.t. } x(0) = \hat{x}(t_s), \quad (4b)$$

$$\dot{x}(t) \in F(x(t), u(t)), \quad t \in [0, T], \quad (4c)$$

$$G(x(t), u(t)) \leq 0, \quad t \in [0, T], \quad (4d)$$

$$G_T(x(T)) \leq 0. \quad (4e)$$

Here,  $\ell : \mathbb{R}^{n_x} \times \mathbb{R}^{n_u} \rightarrow \mathbb{R}$  is the stage cost,  $\ell_T : \mathbb{R}^{n_x} \rightarrow \mathbb{R}$  the terminal cost, and  $G : \mathbb{R}^{n_x} \times \mathbb{R}^{n_u} \rightarrow \mathbb{R}^{n_G}$ ,  $G_T :$

$\mathbb{R}^{n_u} \rightarrow \mathbb{R}^{n_{G_T}}$  collect path and terminal constraints. In the initial constraint (4b)  $\hat{x}(t_s)$  is the real state value obtained at sampling instance  $t_s$ . To apply MPC, (4) needs to be solved at sampling instants  $t_s$  over a receding time horizon. Then, the first part of a control input  $u(t)$ ,  $t \in [t_s, t_{s+1})$  is applied until  $t_{s+1}$ , and the process is repeated. In a discrete-time setting, the control input is usually piecewise constant. Thus, we compute  $u(t) = u_s$ ,  $t \in [t_s, t_{s+1})$ , cf. Sec. III-D. To use (4) for MPC, however, some reformulations are necessary.

### B. Dynamic Complementarity System

To obtain a computationally efficient model of the Filippov inclusion, it is reformulated into a dynamic complementarity system (DCS) and discriminant functions  $g = [g_1, \dots, g_m]$ ,  $g_i : \mathbb{R}^{n_x} \rightarrow \mathbb{R}$  that encode the regions [19]:

$$R_i = \{x \mid g_i(x) < \min_{j \in \{1, \dots, m\}, j \neq i} g_j(x)\}. \quad (5)$$

At any  $(x, u)$ , the Filippov convex multipliers  $\theta \in \mathbb{R}_{\geq 0}^m$  are the solution of the selector LP with  $\theta = (\theta_1, \dots, \theta_m)$  [13], [19]:

$$\min_{\theta} g(x)^\top \theta \quad \text{s.t.} \quad \mathbf{1}^\top \theta = 1, \theta \geq 0. \quad (6)$$

with  $\mathbf{1} = [1, 1, \dots, 1] \in \mathbb{R}^m$ . A detailed derivation of this process is presented in [13]. Introducing Lagrange multipliers  $\lambda \in \mathbb{R}_{\geq 0}^m$  and  $\mu \in \mathbb{R}$ , the KKT conditions are

$$g(x) - \lambda - \mu \mathbf{1} = 0, \quad (7a)$$

$$1 - \mathbf{1}^\top \theta = 0, \quad (7b)$$

$$\theta \geq 0, \mu \geq 0, \theta \perp \mu. \quad (7c)$$

Together with

$$\dot{x} = \sum_{i=1}^m \theta_i f_i(x, u), \quad (8)$$

this defines a DCS in  $(x, \theta, \lambda, \mu)$  that is equivalent to the Filippov model in (3). To facilitate the implementation of an MPC controller, we can now replace (4c) in the OCP by the DCS (7)–(8). Afterwards, we discretize this OCP in time to obtain a finite-dimensional MPCC, which we can efficiently solve using NOSNOC.

### C. Time Discretization and Switch Detection

To discretize the DCS (7)–(8), we utilize the scheme presented in [13]. For ease of exposition, we consider a single control interval  $[T_k, T_{k+1}] \subseteq [0, T]$  with a constant input  $\bar{u}$  and initial value  $x_0$ . We split it into  $N_{\text{FE}}$  finite elements  $[t_n, t_{n+1}]$ , with grid points  $T_k = t_0 < \dots < t_{N_{\text{FE}}} = T_{k+1}$ , with step sizes  $h_n = t_{n+1} - t_n$ . On each element, we apply an  $n_{\text{RK}}$ -stage Runge–Kutta (RK) [12]. Let  $x_n \approx x(t_n)$  be the left state,  $V_n = (v_{n,1}, \dots, v_{n,n_{\text{RK}}})$  the RK-stage derivatives,  $\Theta_n = (\theta_{n,1}, \dots, \theta_{n,n_{\text{RK}}})$  the stage values of the selector, and  $(\Lambda_n, M_n)$  the corresponding Lagrange multipliers in (7). We collect all RK-stage variables for the  $n$ -th finite element in  $Z_n = (x_n, V_n, \Theta_n, \Lambda_n, M_n)$ .

For one element, we can summarize all RK-equations in  $G_{\text{rk}}$ , which then stacks all RK equations for the DCS.

Thus, over  $[T_k, T_{k+1}]$ , we stack  $Z = (Z_0, \dots, Z_{N_{\text{FE}}-1})$  and  $H = (h_0, \dots, h_{N_{\text{FE}}-1})$  to obtain

$$x_{k+1} = F_{\text{std}}(Z), \quad 0 = G_{\text{std}}(Z, H, x_k, \bar{u}), \quad (9)$$

a discrete-time non-smooth map. Where  $G_{\text{std}}$  stacks all computations of the standard RK method over all integration intervals. This discretization is only accurate if the grid points and switching points intersect, which is rare in practice [1].

To address this, switch detection is introduced by making the step sizes  $h_n$  optimization decision variables and augmenting  $G_{\text{std}}$  with cross-complementarity constraints  $0 = G_{\text{cross}}(Z, H, x_k)$  and step equilibration  $0 = G_{\text{eq}}(Z, H, x_k)$ . This enforces a constant active set (i.e., switching mode) within each element by making changes only possible at grid points while keeping the elements equidistant from switching points. For details on the functions  $G_{\text{rk}}$ ,  $G_{\text{std}}$ ,  $G_{\text{cross}}$  and  $G_{\text{eq}}$ , cf. [12, Sec. III].

With the length constraint  $\sum_{n=0}^{N_{\text{FE}}-1} h_n = T_{k+1} - T_k$ , the full finite element step with switch detection is [13]

$$x_{k+1} = F_{\text{fesd}}(Z), \quad 0 = G_{\text{fesd}}^k(Z, H, x_k, \bar{u}),$$

$$G_{\text{fesd}}^k(Z, H, x_k, \bar{u}) := \begin{bmatrix} G_{\text{std}}(Z, H, x_k, \bar{u}) \\ G_{\text{cross}}(\Theta, \Lambda) \\ G_{\text{eq}}(H, \Theta, \Lambda) \\ \sum_{n=0}^{N_{\text{FE}}-1} h_n - T_{k+1} + T_k \end{bmatrix}, \quad (10)$$

which serves as an integrator with exact switch detection in a time-discretized OCP, described in the next section.

#### D. Discrete-time MPC subproblem as an MPCC

To write the discretized version of the OCP (4), we consider  $N_{\text{CI}}$  control intervals of equal length and define  $\mathbf{x} = (x_0, \dots, x_{N_{\text{CI}}})$  be the states at control grid nodes,  $\mathbf{u} = (u_0, \dots, u_{N_{\text{CI}}-1})$  the control inputs,  $\mathbf{Z} = (Z_0, \dots, Z_{N_{\text{CI}}-1})$  the collection of all internal variables, and  $\mathcal{H} = (H_0, \dots, H_{N_{\text{CI}}-1})$  all step sizes stacked per stage as introduced above. Thus, the time-discrete version of the OCP (4) can now be written as

$$\min_{\mathbf{x}, \mathbf{u}, \mathbf{Z}, \mathcal{H}} \sum_{k=0}^{N_{\text{CI}}-1} \hat{\ell}_k(x_k, Z_k, H_k, u_k) + \hat{\ell}_T(x_{N_{\text{CI}}}) \quad (11a)$$

$$\text{s. t. } x_0 = x(t_s), \quad (11b)$$

$$G_T(x_{N_{\text{CI}}}) \leq 0, \quad (11c)$$

$$\forall k \in (0, \dots, N_{\text{CI}} - 1) : \\ x_{k+1} = F_{\text{fesd}}(Z_k), \quad (11d)$$

$$G_{\text{fesd}}^k(Z_k, H_k, x_k, u_k) = 0, \quad (11e)$$

$$G(x_k, u_k) \leq 0, \quad (11f)$$

where  $\hat{\ell}_k$  and  $\hat{\ell}_T$  define the time-discretized cost (4a). The FDI (4c) is replaced by its time-discretization (10), and the path constraints (4d) are evaluated at the control grid points yielding (11f). Because  $G_{\text{fesd}}$  embeds complementarity from the KKT conditions of the selector LP (cf. (7c)) and cross-complementarity constraints, (11) is a mathematical program

with complementarity constraints, which can be written in compact form

$$\min_w f(w) \quad (12a)$$

$$\text{s. t. } h(w) \geq 0, \quad (12b)$$

$$0 \leq w_1 \perp w_2 \geq 0, \quad (12c)$$

for a suitable partition  $w = (w_0, w_1, w_2) \in \mathbb{R}^{n_w}$  of all decision variables [12]. We solve the MPCC via a homotopy, whereby NOSNOC supports, replacing the bilinear orthogonality by  $w_1^\top w_2 = \sigma_i$  (smoothing) or by  $w_1^\top w_2 \leq \sigma_i$  (relaxation) and solving a sequence of smooth NLPs with a parameter  $\sigma$  driven to zero. Under standard assumptions, letting  $\sigma_i \rightarrow 0$  recovers an MPCC solution [20].

#### IV. EXPERIMENTAL EVALUATION

To demonstrate our approach in real-time, we consider the three-tank system shown in Fig. 1. This setup consists of three similarly sized tanks and two pumps, feeding into the top of tanks 1 and 3. Each tank is equipped with a bottom-mounted level sensor and drains to the outside of the system. Furthermore, there are connections between tanks 1 and 2, as well as tanks 2 and 3. Each of these connections and drains is equipped with a continuous differential valve. The tank base area  $A$  as well as all cross-sectional areas  $q_i$ , with  $i \in \{1, 2, d1, d2, d3\}$  are denoted in Table I and can be changed between these values and 0 continuously via the valves. The parameters with subscripts d are drains, and the others are tank connections. The full piecewise-smooth model of the system can thus be written as in (13), where  $g = 9.81 \text{ ms}^{-2}$  is the gravitational acceleration, the heights are the states  $x = [x_1, x_2, x_3]^\top$ . In (13), the equal-height sets  $x_1 = x_2$  and  $x_2 = x_3$  are part of the switching set and thus pose a challenge regarding the square root  $f_{\text{sqr}}(x) = \sqrt{x}$ , which are defined only for  $x \geq 0$  and are not Lipschitz at  $x = 0$ . Consequently,  $f'_{\text{sqr}}(x) = \frac{1}{2\sqrt{x}}$  and  $f''_{\text{sqr}}(x) = -\frac{1}{4}x^{-3/2}$  blow up as  $x \rightarrow 0$ , which yields unbounded derivatives near the equal-level sets at the region boundaries. A low complexity solution is to add regions symmetrically around the borders  $\partial R_i$  and approximate the behavior linearly with e.g.  $f_{\text{lin, sqrt}} = q\sqrt{\frac{2g}{k}}(x_2 - x_1)$ , where  $k := \|x_1 - x_2\|$  is the euclidean distance to the border. The larger the chosen  $k$ , the larger the model mismatch becomes. Adding these regions around the borders increases the number of regions from 4, as seen in (13) to 9 if we only consider the connections and not include the drains. We do this to avoid the proliferation of modes (here  $m = 3^2 \cdot 2^3 = 72$ ), which would greatly inflate problem size. To remedy this, we can shift the feasible set away from the scenarios where the root-terms of the drains approach 0, by adjusting the lower bound to, e.g., 0.1 cm. As a further safeguard, we introduce max functions under the remaining square-root terms to ensure positivity, i.e., clipping its argument to some minimum value  $e$ . This is done to prevent numerical issues in evaluating the dynamic equations. These states need to be derived from the voltage signals produced by the level sensors, which is done by the

$$\dot{x}_1 = \frac{1}{A} \begin{cases} u_1 - q_1 \sqrt{2g(x_1 - x_2)} - q_{d1} \sqrt{2gx_1}, & x_1 > x_2, \\ u_1 + q_1 \sqrt{2g(x_2 - x_1)} - q_{d1} \sqrt{2gx_1}, & x_1 < x_2, \end{cases} \quad (13a)$$

$$\dot{x}_2 = \frac{1}{A} \begin{cases} q_1 \sqrt{2g(x_1 - x_2)} + q_2 \sqrt{2g(x_3 - x_2)} - q_{d2} \sqrt{2gx_2}, & x_1 > x_2 \wedge x_3 > x_2, \\ -q_1 \sqrt{2g(x_2 - x_1)} + q_2 \sqrt{2g(x_3 - x_2)} - q_{d2} \sqrt{2gx_2}, & x_1 < x_2 \wedge x_3 > x_2, \\ q_1 \sqrt{2g(x_1 - x_2)} - q_2 \sqrt{2g(x_2 - x_3)} - q_{d2} \sqrt{2gx_2}, & x_1 > x_2 \wedge x_3 < x_2, \\ -q_1 \sqrt{2g(x_2 - x_1)} - q_2 \sqrt{2g(x_2 - x_3)} - q_{d2} \sqrt{2gx_2}, & x_1 < x_2 \wedge x_3 < x_2, \end{cases} \quad (13b)$$

$$\dot{x}_3 = \frac{1}{A} \begin{cases} u_2 - q_2 \sqrt{2g(x_3 - x_2)} - q_{d3} \sqrt{2gx_3}, & x_3 > x_2, \\ u_2 + q_2 \sqrt{2g(x_2 - x_3)} - q_{d3} \sqrt{2gx_3}, & x_3 < x_2, \end{cases} \quad (13c)$$



Fig. 1. Image of the three-tank-system used in the experiments

following equations

$$\begin{aligned} x_1 &= 29.942 \text{ cm} - 3.344 \text{ cmV}^{-1} \cdot U_{1,s}, \\ x_2 &= 29.449 \text{ cm} - 3.326 \text{ cmV}^{-1} \cdot U_{2,s}, \\ x_3 &= 28.948 \text{ cm} - 3.330 \text{ cmV}^{-1} \cdot U_{3,s}, \end{aligned}$$

where  $U_{1,s}$ ,  $U_{2,s}$ , and  $U_{3,s}$  are the voltages output by the sensors. The control inputs  $[u_1, u_2]$  are the flow rates driven by the pumps, which are themselves voltage-controlled. Therefore, the inputs are defined implicitly by the equations

$$\begin{aligned} u_1 &= 64.672 \text{ cm}^3 \text{s}^{-1} + 6.186 \text{ cm}^3 \text{V}^{-1} \text{s}^{-1} \cdot U_{1,p}, \\ u_2 &= 64.672 \text{ cm}^3 \text{s}^{-1} + 6.186 \text{ cm}^3 \text{V}^{-1} \text{s}^{-1} \cdot U_{2,p}, \end{aligned}$$

where  $U_{1,p}$  and  $U_{2,p}$  are the input voltages of the pumps.

The control scheme is implemented via MATLAB 2023b using NOSNOC [12] for modeling the system, formulating and discretizing the OCP, and solving the resulting MPCC in an MPC loop. NOSNOC uses CasADi [16] for generating the necessary functions used to solve the OCP. We use the Data Acquisition Toolbox in order to connect to the NI USB 6341 I/O card [21], which is used for the interface to the physical system. After installing the appropriate support package, the card was configured in MATLAB, defining its inputs, outputs, and sampling rate. The signal ranges of the card and the amplifier are limited to  $[-10 \text{ V}, 10 \text{ V}]$ . For the controller, we use the bounds shown in Table II. We use a state-dependent quadratic stage cost function  $\ell(x) = x^\top Q x$ , where  $Q$  is the identity matrix, and no terminal cost, with a prediction horizon  $T = 50 \text{ s}$ , with  $N_{CI} = 10$  control intervals

TABLE I. Values of the tank base area  $A$  and all cross-sectional areas  $q_i$

Parameter	Cross-sectional area (cm <sup>2</sup> )
$A$	153.941
$q_1$	0.218
$q_2$	0.228
$q_{d1}$	0.373
$q_{d2}$	0.427
$q_{d3}$	0.331

TABLE II. Values of the state and input bounds

Bound	Lower	Upper
$x_1, x_2, x_3$	0.1 cm	60 cm
$u_1$	0 cm <sup>3</sup> s <sup>-1</sup>	125 cm <sup>3</sup> s <sup>-1</sup>
$u_2$	0 cm <sup>3</sup> s <sup>-1</sup>	137 cm <sup>3</sup> s <sup>-1</sup>

and a second-order Runge-Kutta method. The number of finite elements  $N_{FE}$  was chosen as 2. For the homotopy, we chose a superlinear update rule with  $(\sigma_1, \sigma_2, \sigma_3, \sigma_4) = (1, 10^{-1}, 10^{-3}, 10^{-9})$ . Further, we warm start the solver with a shifted form of the previous solution.

#### A. Scenario Definition

In all scenarios, our goal is to drive the system to a defined operating point. Note that not all operating points are reachable, as our system is underactuated, having no direct control for the level in tank 2. For the regions, we consider the regions of the real unaugmented model (13) given as

$$\begin{aligned} R_1 &:= \{x \in \mathbb{R}^3 \mid x_1 < x_2, x_2 > x_3\}, \\ R_2 &:= \{x \in \mathbb{R}^3 \mid x_1 < x_2, x_2 < x_3\}, \\ R_3 &:= \{x \in \mathbb{R}^3 \mid x_1 > x_2, x_2 > x_3\}, \\ R_4 &:= \{x \in \mathbb{R}^3 \mid x_1 > x_2, x_2 < x_3\}. \end{aligned}$$

The valve in the drain of tank 2 is closed in all scenarios, meaning  $q_{d2} = 0$ , and we chose  $k = 1$  and  $e = 1e^{-6}$ .

a) *Scenario 1:* Tank 1 should be driven to 20 cm, tank 2 to 15 cm, and tank 3 20 cm. After 100 s, we switch the operating point values of tanks 1 and 3, and after 200 s, we switch them back.

b) *Scenario 2:* We investigate how well the MPC with the augmented model works for a model mismatch. For this, we use a similar setup as for Scenario 1 but reduce the diameter of the connection valves to 70 %. The goal is to reach a operating point for tank 1 of 25 cm, tank 2 of 20 cm, and tank 3 of 15 cm, switching the operating points of tank 1 and 3 after 95 s and 165 s.

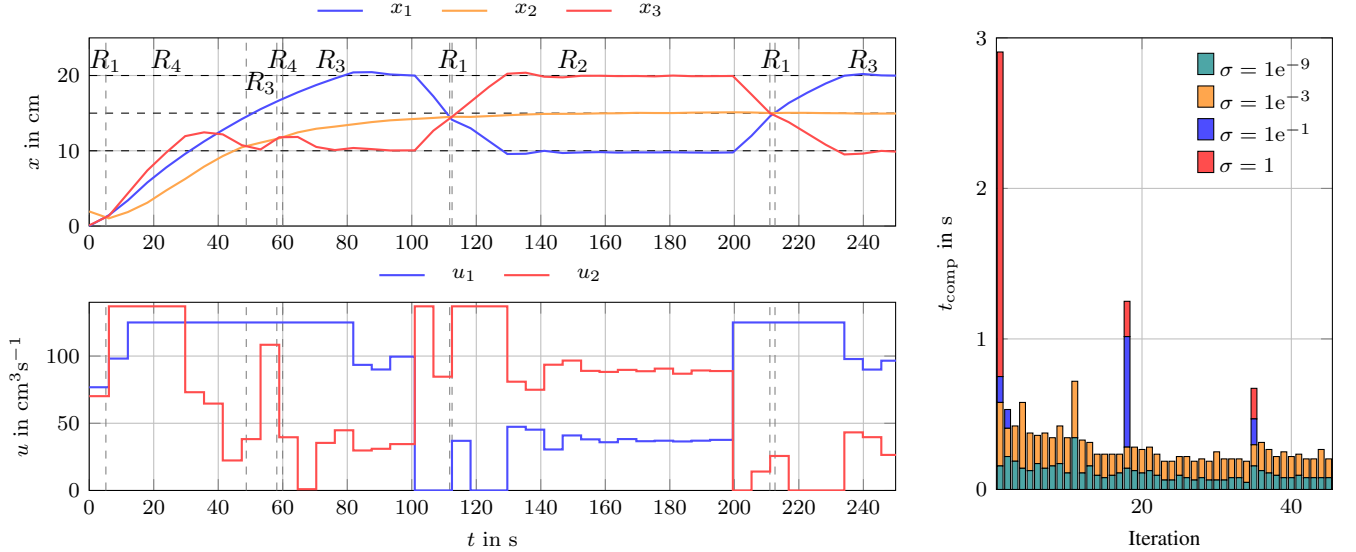


Fig. 2. Scenario 1: Tank heights are shown on the top and inflows on the bottom. References show as dashed horizontal lines and region switches as dashed vertical lines. Detailed computation times are shown on the right (including CPU times for each NLP solve in the MPCC homotopy).

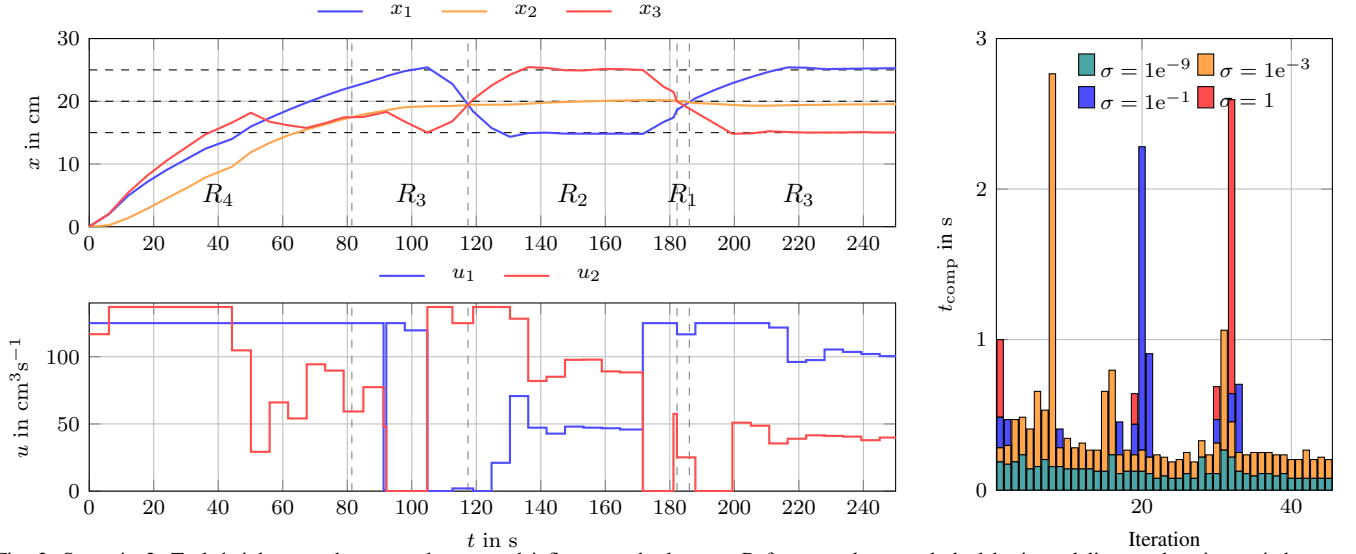


Fig. 3. Scenario 2: Tank heights are shown on the top and inflows on the bottom. References show as dashed horizontal lines and region switches as dashed vertical lines. Detailed computation times are shown on the right (including CPU times for each NLP solve in the MPCC homotopy).

### B. Scenario 1: Reference cascade

Figure 2 shows the closed-loop trajectories, references, and the computation times for each control interval. The system undergoes multiple mode transitions in the first control interval since a direct transition  $R_1 \rightarrow R_4$  is impossible in both the unaugmented model (13) and the augmented model. The tank levels rise to their setpoints, with only tank 1 showing an initial overshoot, which takes several control intervals to settle, but does not recur at the setpoint switches. At  $t = 100$  s the controller executes the mirrored setpoint (swapping tank 1 and 3), and at  $t = 200$  s it returns to the original target. Deviations occur mainly around the switching instant. Tank 2 remains at the setpoint despite the switching of the reference. Computation times peak near switching events and are otherwise lower during near-steady operation.

### C. Scenario 2: Model-mismatch

In Figure 3, we show the state and input trajectories during the experimental run with model-mismatch. The tank levels

rise from the initially empty tanks to the setpoints. Tank 3 shows a larger overshoot than in Scenario 1. Tank 2 does not settle to the set point and shows a small oscillating behavior around the reference.

As in the first scenario, the reference switches are performed by MPC with little over- and undershoot despite forcing region switches. The computation time is also comparable and similarly peaks during setpoint switches. These peaks are more pronounced and span several control intervals. The homotopy iterations also remain at higher  $\sigma$  values for several control intervals during these peaks. However, in both cases the computation times stay below the sampling time of 5 s, rendering the MPC real-time feasible.

### D. Discussion

The experiments indicate that non-smooth MPC achieves real-time capable control of a switching three-tank process while preserving mode consistency. Across scenarios, reference changes are tracked without unwanted behavior at

region borders. Hence, the discrete dynamics remain faithful to the Filippov model and deliver reliable sensitivities.

Despite the multiple mode changes in the first control interval in Scenario 1, trajectories converge to the operating point. The brief overshoot of tank 1 vanishes at later setpoint swaps, consistent with improved warm starts and a closer proximity to the new targets, which reduces aggressive transients likely due to better active-set guesses. The overshoot might also be the result of the interconnected dynamics and might be needed to drive tank 2 to its reference point.

Because tank 2 is not directly actuated, the feasibility of operating points depends on the inter-tank flow balance. In Scenario 1, tank 2 settles at its target. Because of the connection mismatch in Scenario 2, tank 2 exhibits a small steady error and light oscillations, while tank 3 shows a larger overshoot. This could be addressed via an offset-free MPC scheme using a disturbance model [22], [23]. Nevertheless, constraint satisfaction and correct mode sequencing are preserved, and the reference swaps are performed successfully.

To regularize non-Lipschitz square-root terms near zero, we combined a narrow linear region around the border with clipping via  $\max(e, \cdot)$  and a small shift of the state lower bounds. This augmentation improves numerical robustness. The observed tracking quality suggests that, for the exercised operating points, this modified model is sufficient.

Computation times peak at setpoint changes and near major mode updates, then settle at lower values during near-steady operation. The peak can be explained by the new reference forcing a cold start, and that several homotopy steps are needed until the active set stabilizes, during which the  $\sigma$  remains comparatively large. With the chosen schedule for  $\sigma$  and warm starts of states, inputs, and multipliers, the controller remains real-time capable in both scenarios.

## V. CONCLUSION AND OUTLOOK

We presented a non-smooth MPC approach based on the NOSNOC framework, which combines Filippov/DCS modeling, FESD discretization, and homotopy-based MPCC solving. We validate its performance for switching systems on a real three-tank system.

The methodology maintains the switching behavior, aligns discretization with mode transitions, and avoids mixed-integer formulations. In the laboratory setup, the controller preserves mode sequencing, handles sliding and boundary behavior consistently, and achieves accurate reference tracking while satisfying constraints. Computation remains within real-time limits, and the approach shows robustness to structural model mismatch, indicating practical deployability of non-smooth MPC based on continuous optimization.

A limitation stems from the computational effort associated with solving MPCCs, which restricts achievable sampling rates and system complexity. Future directions should focus on accelerating the optimization pipeline through tailored MPCC solvers, improved homotopy strategies, and structure-exploiting numerical techniques. Additional extensions include applying the methodology to more complex non-smooth systems, such as mechanical contact or process

systems with richer logic, and integrating offset-free, robust, or stochastic MPC formulations into the non-smooth setting.

## REFERENCES

- [1] V. Acary and B. Brogliato, *Numerical methods for nonsmooth dynamical systems: applications in mechanics and electronics*. Springer Science & Business Media, 2008.
- [2] S. Lucia, M. Kögel, P. Zometa, D. E. Quevedo, and R. Findeisen, "Predictive control, embedded cyberphysical systems and systems of systems – a perspective," *Annu. Rev. Control*, vol. 41, 2016.
- [3] J. Rawlings, D. Mayne, and M. Diehl, *Model predictive control: theory, computation, and design*. Nob Hill Publishing, 2017.
- [4] A. Bemporad and M. Morari, "Control of systems integrating logic, dynamics, and constraints," *Automatica*, vol. 35, no. 3, 1999.
- [5] A. Bemporad, W. M. H. Heemels, and B. De Schutter, "On hybrid systems and closed-loop MPC systems," *IEEE Trans. Automat. Contr.*, vol. 47, no. 5, 2002.
- [6] J. Villa, M. Duque, A. Gauthier, and N. Rakoto-Ravalontsalama, "MLD control of hybrid systems: application to the three tank benchmark problem," in *Conf. Proc. IEEE Int. Conf. Syst. Man. Cybern.*, vol. 1, 2003.
- [7] M. Lazar, W. Heemels, S. Weiland, and A. Bemporad, "Stabilizing model predictive control of hybrid systems," *IEEE Trans. Automat. Contr.*, vol. 51, no. 11, 2006.
- [8] H. Yaakoubi, H. Rezk, M. Al-Dhaifallah, and J. Haggège, "MLD-MPC approach for three-tank hybrid benchmark problem," *Comput. Mater. Contin.*, vol. 75, no. 2, 2023.
- [9] D. Liberzon, *Switching in systems and control*. Springer, 2003, vol. 190.
- [10] A. Nurkanović, S. Albrecht, and M. Diehl, "Limits of MPCC formulations in direct optimal control with nonsmooth differential equations," in *2020 Eur. Control Conf. (ECC)*, 2020.
- [11] D. E. Stewart and M. Anitescu, "Optimal control of systems with discontinuous differential equations," *Numer. Math. (Heidelb.)*, vol. 114, no. 4, 2010.
- [12] A. Nurkanović and M. Diehl, "nosnoc: A software package for numerical optimal control of nonsmooth systems," *IEEE Control Syst. Lett.*, vol. 6, 2022.
- [13] A. Nurkanović, M. Sperl, S. Albrecht, and M. Diehl, "Finite elements with switch detection for direct optimal control of nonsmooth systems," *Numer. Math. (Heidelb.)*, 2024.
- [14] A. Nurkanović, A. Pozharskiy, and M. Diehl, "Solving mathematical programs with complementarity constraints arising in nonsmooth optimal control," *Vietnam J Math.*, vol. 53, 2024.
- [15] A. Nurkanović, A. Pozharskiy, J. Frey, and M. Diehl, "Finite elements with switch detection for numerical optimal control of nonsmooth dynamical systems with set-valued Heaviside step functions," *Nonlinear Anal.: Hybrid Syst.*, vol. 54, 2024.
- [16] J. A. E. Andersson, J. Gillis, G. Horn, J. B. Rawlings, and M. Diehl, "CasADi – A software framework for nonlinear optimization and optimal control," *Math. prog. comp.*, vol. 11, no. 1, 2019.
- [17] A. Wächter and L. T. Biegler, "On the implementation of an interior-point filter line-search algorithm for large-scale nonlinear programming," *Math. Program.*, vol. 106, no. 1, Mar. 2006.
- [18] A. F. Filippov, "Differential equations with discontinuous right-hand side," *Matematicheskii sbornik*, vol. 93, no. 1, 1960.
- [19] D. Stewart, "A high accuracy method for solving odes with discontinuous right-hand side," *Numer. Math. (Heidelb.)*, vol. 58, no. 1, 1990.
- [20] T. Hoheisel, C. Kanzow, and A. Schwartz, "Theoretical and numerical comparison of relaxation methods for mathematical programs with complementarity constraints," *Math. Program.*, vol. 137, no. 1, 2013.
- [21] NI/Emerson, "USB-6341 specifications," accessed: Oct. 24, 2025. [Online]. Available: <https://www.ni.com/docs/de-DE/bundle/usb-6341-specs/page/specs.html>
- [22] M. Morari and U. Maeder, "Nonlinear offset-free model predictive control," *Automatica*, vol. 48, no. 9, 2012.
- [23] G. Pannocchia, "Offset-free tracking MPC: A tutorial review and comparison of different formulations," in *2015 Eur. Control Conf. (ECC)*, 2015.